

## Hydrogen-Bond Donor-Acceptor Imbalance in Low-Frequency Terahertz Water Spectra

Lilian Najm Alsayed<sup>1</sup>, Florian Pabst<sup>2</sup>, Giuseppe Cassone<sup>3</sup>, Ali Hassanali<sup>2</sup>, Fabio Novelli<sup>1,\*</sup>

<sup>1</sup>School of Physics and Astronomy, Faculty of Engineering and Physical Sciences, University of Southampton, UK

<sup>2</sup>CMSP, The Abdus Salam Centre for Theoretical Physics, 34151 Trieste, Italy

<sup>3</sup>Institute for Chemical-Physical Processes, National Research Council of Italy, viale Ferdinando Stagno d'Alcontres 37, 98158 Messina, Italy

\*F.Novelli@soton.ac.uk

*The low-frequency dielectric response of liquid water is commonly described by a dominant Debye relaxation together with additional faster contributions whose microscopic origin remains debated. Here we show that the dielectric function of water between 0.14 and 1.21 THz can be represented by a collective Debye relaxation plus a Drude-Smith term constrained to the zero-dc-conductivity limit. The Drude-Smith spectral weight increases upon heating pure H<sub>2</sub>O from 20 °C to 50 °C and decreases upon isotopic substitution (D<sub>2</sub>O at 20 °C vs. H<sub>2</sub>O at 20 °C). Molecular dynamics simulations including nuclear quantum effects show correlated changes in the population of water molecules with unequal numbers of donated and accepted hydrogen-bonds. Ab-initio-based spectra calculations further indicate that the ~0.1-1 THz response contains both nuclear-motion and explicit electronic-polarisation/charge-redistribution contributions. We therefore interpret the excess low-frequency THz response as a localised, mixed nuclear-electronic dielectric response correlated with transient donor-acceptor imbalance in the hydrogen-bond network.*

One of the key properties of a hydrogen bond is the electronic charge transfer between donor and acceptor molecules, leading to partial covalent character<sup>1</sup>. This charge transfer term can contribute to ~20-40% of the bond energy in a water dimer<sup>2,3</sup> and arises due to a small charge delocalisation, of approximately 0.02 electrons per bond<sup>4-6</sup>, involving the acceptor on one water molecule (oxygen lone-pair orbitals) and the nearby donor molecule (antibonding  $\sigma_{OH}^*$  orbital)<sup>7</sup>. It has been suggested that such charge-transfer processes may affect the intensity<sup>8-10</sup> and peak positions<sup>11,12</sup> of the vibrational spectra of liquid water, contribute to electronic polarizability<sup>13</sup>, and assist the stabilisation of aqueous hydrophobic interfaces<sup>14,15</sup>.

In the simplest, qualitative terms, if one water molecule in the liquid phase forms four hydrogen bonds, two donated and two accepted, the charge redistribution associated with the two accepted bonds is expected to compensate the charge redistribution associated with the two donated bonds. However, a substantial fraction of water molecules in the liquid phase are transiently under- or over-coordinated at any instant of time, and several of these non-tetrahedral environments involve an imbalance between the number of donated and accepted hydrogen bonds<sup>16-18</sup>. For molecules with such an instantaneous imbalance, the local nuclear network structure, intermolecular charge redistribution, and polarization environment are asymmetric. This local asymmetry, which encompasses both nuclear and electronic degrees of freedom, could contribute to dielectric fluctuations with characteristic spectroscopic signatures.

In simple conductors, the Drude model describes the spectroscopic response in terms of free carriers characterized by a plasma frequency and a scattering time. Whenever the field-induced current is spatially confined, for example in nanostructured or disordered media<sup>19-21</sup>, the Drude description becomes inadequate, and the semi-empirical Drude-Smith formalism can be used<sup>22-28</sup>. In the original formulation<sup>29</sup>, Smith introduced a “backscattering” parameter  $c$  to account for the possibility that the carrier velocity reverses direction before decaying. For example, in a nanomaterial, the carriers could bounce off the boundary and reverse direction of motion<sup>19-21</sup>. Cocker *et al.*<sup>30</sup> later performed Monte Carlo simulations and suggested that the Drude-Smith response stems from diffusive restoring currents, implying that  $c$  should be interpreted as a localisation parameter. Finally, while Kužel and Němec<sup>31</sup> stressed that the Drude-Smith is an effective model that requires further microscopic validation before interpreting its parameters, Chen and Marcus<sup>32</sup> derived it under the assumption of non-Markovian transport, that is, whenever the transport cannot be written as a function of a single temporal variable but depends on the history of the charge interactions.

While plasma frequency and scattering time are present in both Drude and Drude-Smith models, the  $c$  parameter determines the qualitative transport regime. For  $c = 0$  there is no backscattering or charge localisation, and the Drude-Smith is identical to the Drude model with long-range carrier transport and sizeable conductivity at zero frequency. For  $c = -1$  the localisation is complete, the static conductivity is reduced to zero, and no long-range transport is possible. As pure liquid water has zero dc conductivity stemming from the motion of free electronic carriers, here we explore whether its low-frequency response could be in part described by a Drude-Smith term wherein  $c$  is fixed to  $-1$ .

Liquid water displays a broad spectroscopic feature centred at  $\sim 20$  GHz and extending into the terahertz (THz) frequency range, which often fits a Debye function with a reorientation time constant of 8-10 ps<sup>33-37</sup>. Even though the Debye function originally described the time it takes for pre-aligned and non-interacting dipoles to randomise after the driving electric field is turned off, it works surprisingly well for a network-forming liquid such as water. Above about 0.2 THz, however, a single Debye term is insufficient to describe the dielectric function of water, and at least one additional contribution is required<sup>38,39</sup>. While it could be preferable to use a broad distribution rather than one additional discrete process<sup>40,41</sup>, several fit procedures were proposed by adding either a log-normal function describing excess vibrational states akin to the boson peak in glass-forming materials<sup>42</sup>, Lorentzian-shaped Raman responses owing to the fact that a water molecule lacks a centre of inversion<sup>43</sup>, or additional Debye function(s) with faster reorientation time constants of 0.1-1 ps, qualitatively associated with water molecules with weaker hydrogen bonds<sup>44-47</sup>. The latter description of the THz response of water with two Debye functions is widely used. However, while the main Debye relaxation can be associated with collective dipolar reorientation of hydrogen-bonded water molecules<sup>48-50</sup>, the microscopic description of the faster Debye term(s) remains unclear. The faster Debye-type processes have been assigned to transient, weakly or non-hydrogen-bonded structures, but display small and inconsistent temperature and isotope dependences<sup>33-37</sup>.

Here we show that a fit including the main Debye term with 8-10 ps time-constant, and one Drude-Smith component with  $c = -1$ , can be used to describe the dielectric response of liquid water between about 0.14 and 1.21 THz. We recorded spectra of pure water at 20 °C, H<sub>2</sub>O at 50 °C, and heavy water at 20 °C. We found that the Drude-Smith effective spectral weight increases when the hydrogen-bond network is weakened by heating and decreases when it is strengthened by deuteration. Dedicated neural-network-based molecular dynamics simulations revealed correlations between such spectral responses and the populations of water molecules with unequal numbers of donated and accepted hydrogen bonds. These results introduce a novel empirical approach to fit the low-frequency THz spectra of aqueous materials, wherein the obtained fit parameters correlate with average structural properties of the hydrogen-bond network. Finally, *ab-initio*-based calculations indicate that there are contributions from both the nuclear and electronic degrees of freedom in the low-frequency range: the low-frequency THz features are consistent with contributions from nuclear-network rearrangements, intermolecular charge redistribution, and polarisation effects associated with asymmetries in local hydrogen-bonding patterns.

The dielectric function of liquid water at THz frequencies and 20 °C was tabulated by collating multiple previous reports, see Table 1 in ref.<sup>51</sup>. The corresponding refractive index ( $n_{wat}$ ) and extinction coefficient ( $k_{wat}$ ) are shown as blue and red circles in Figure 1, respectively.

We performed measurements with intense terahertz time-domain spectroscopy to maximise the signal transmitted by an opaque sample such as a half-millimetre thick aqueous layer<sup>51,52</sup>. Pure milli-Q liquid water at  $20 \pm 0.05$  °C was used as reference to estimate the dielectric functions of pure milli-Q liquid water at  $50 \pm 0.05$  °C and of  $>99\%$ -pure D<sub>2</sub>O at  $20 \pm 0.05$  °C. The experimental results together with the estimation procedure are reported in the Supplementary

Information (SI). The corresponding values of refractive index and extinction coefficient are displayed in Figure 2.

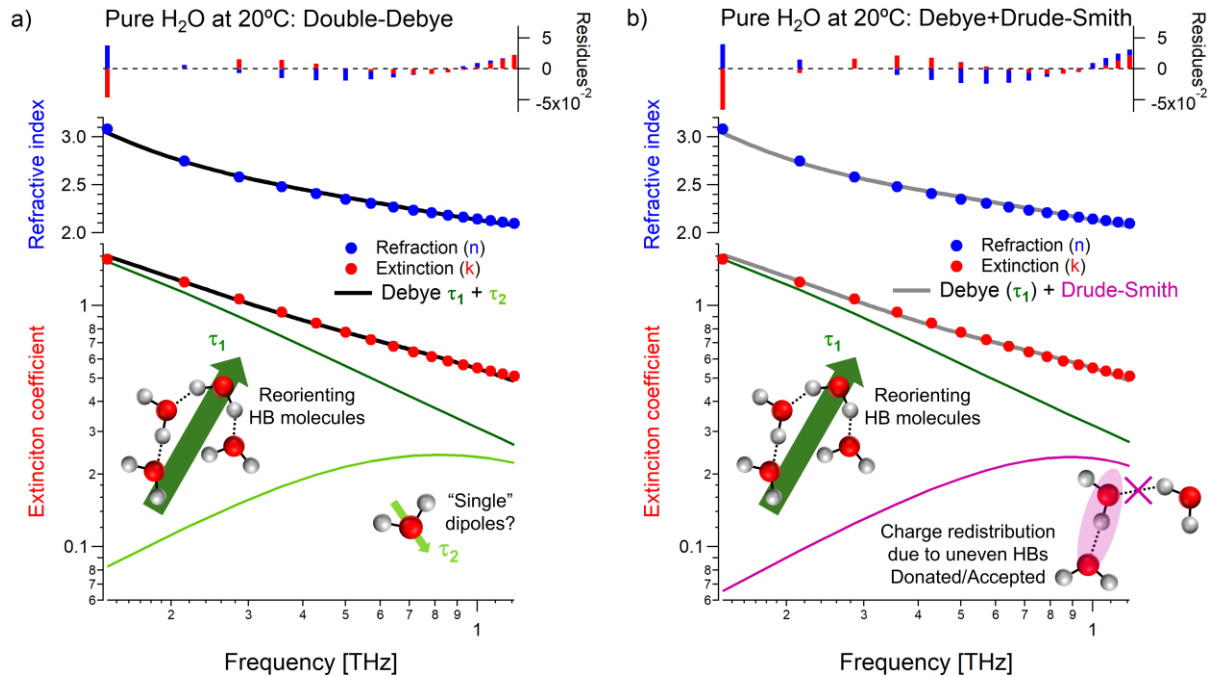


**Figure 1.** Fitting the low-frequency THz dielectric function of liquid water at 20 °C estimated from previous reports<sup>51</sup>. The fit residues are shown on top, the real part of the refractive index of water is reported in blue, and the extinction coefficient in red. a) The usual double-Debye fit (black lines) is consistent with two reorientation mechanisms with time-constants of about 8 ps and 200 fs, respectively. While the slower and dominant Debye process is consistent with dipole reorientations of groups of hydrogen-bonded water molecules, the faster and weaker process has been ascribed to water molecules characterized by weaker or distorted hydrogen bonding. b) A single Debye plus Drude-Smith fit (grey lines) produces comparable results. While the slower and dominant Debye process remains, the higher-frequency response is empirically consistent with localised dielectric response associated with imbalanced donor/acceptor hydrogen-bond environments.

We fit the dielectric functions to the usual double Debye approach or a single Debye plus Drude-Smith: the equations used are reported in the SI. The best fit results are listed in Table 1 and Table 2, respectively. The uncertainties correspond to the fit errors for H<sub>2</sub>O at 20 °C and to 95% confidence interval (CI) from 15 repeated measurements for H<sub>2</sub>O at 50 °C and D<sub>2</sub>O at 20 °C. To estimate the fit quality, we calculated the sum of the absolute differences between the fit results and the original data. We divided this sum by the average response between 0.14 and 1.21 THz. In other words, we calculated  $\bar{n}_{res} = \sum_{\nu} |n_{res}(\nu)| / \sum_{\nu} n(\nu)$  for the real part of the refractive index, where each residue  $n_{res}(\nu)$  is equal to the difference between the data and the fit at frequency  $\nu$ . Likewise, for the extinction coefficient we used  $\bar{k}_{res} = \sum_{\nu} |k_{res}(\nu)| / \sum_{\nu} k(\nu)$ . The results are summarised in Table 1 and Table 2.

We initially performed a fit of the dielectric function of pure water at 20 °C with the standard double-Debye and compared it with the results of a single Debye plus Drude-Smith. The results are reported in Figure 1a and Figure 1b, respectively. The black lines are the fit

results of the double-Debye fit; the grey ones are Debye plus Drude-Smith results. The two components of the extinction coefficient are sketched at the bottom with the usual, main Debye-type reorientation (dark green in Figure 1) dominating the response at lower THz frequencies. The remaining “bump at higher frequencies” can be represented by either a second Debye term (light green in Figure 1a) or the Drude-Smith component (purple in Figure 1b). As shown on top of Figure 1, in Table 1, and in Table 2, the magnitude of the residuals of the Debye plus Drude-Smith fit are comparable to the ones obtained with the well-established double-Debye approach.

**Table 1.** Fit results with the standard double Debye fit. The static dielectric constants ( $\epsilon_S$ ) were fixed to literature values<sup>53–55</sup>.  $\epsilon_d$  is the first Debye term (sometimes labelled with  $\epsilon_1$ ),  $\epsilon_\infty$  the dielectric constant at higher frequencies,  $\tau_1$  (sometimes labelled with  $\tau_D$ ) and  $\tau_2$  are the reorientation time-constants of the first and second Debye terms, respectively.

	H <sub>2</sub> O at 20 °C	H <sub>2</sub> O at 50 °C	D <sub>2</sub> O at 20 °C
$\epsilon_S$	80.2	69.9	79.8
$\epsilon_d$	$5.57 \pm 0.07$	$5.37 \pm 0.07$	$5.32 \pm 0.07$
$\epsilon_\infty$	$3.53 \pm 0.06$	$3.43 \pm 0.07$	$3.35 \pm 0.06$
$\tau_1$ [ps]	$8.72 \pm 0.09$	$4.71 \pm 0.04$	$11.02 \pm 0.13$
$\tau_2$ [fs]	$219 \pm 13$	$189 \pm 13$	$222 \pm 13$
$\bar{n}_{\text{res}}$ [%] ; $\bar{k}_{\text{res}}$ [%]	0.6 ; 1.4	0.4 ; 1.0	0.6 ; 1.6

**Table 2.** Fit results with the single Debye plus Drude-Smith (bottom). The static dielectric constants were fixed to literature values<sup>53–55</sup>. The  $c$  parameter was locked to a value equal to  $-1$  to account for full localisation<sup>20,30</sup>.  $\omega_P$  is the effective spectral weight parameter and  $\tau$  the effective scattering time.

	H <sub>2</sub> O at 20 °C	H <sub>2</sub> O at 50 °C	D <sub>2</sub> O at 20 °C
$\epsilon_S$	80.2	69.9	79.8
$\epsilon_\infty$	$3.87 \pm 0.03$	$3.77 \pm 0.04$	$3.70 \pm 0.01$
$\tau_1$ [ps]	$8.50 \pm 0.05$	$4.66 \pm 0.02$	$10.77 \pm 0.13$
$c$	-1	-1	-1
$\omega_P$ [rad/ps]	$11.16 \pm 0.31$	$12.13 \pm 0.44$	$10.60 \pm 0.11$
$\tau$ [fs]	$110 \pm 3$	$100 \pm 4$	$114 \pm 1$
$\bar{n}_{\text{res}}$ [%] ; $\bar{k}_{\text{res}}$ [%]	0.7 ; 1.6	0.5 ; 1.0	0.8 ; 1.8

Having demonstrated that the Debye plus Drude-Smith fit can reproduce the dielectric response of water, we tested whether it gives reasonable results under different hydrogen-bond-network conditions, i.e., when the network is more disordered due to a temperature increase, or when it is stronger, as in D<sub>2</sub>O<sup>11</sup>. In Figure 2 we display the refractive (blue) and extinction (red) coefficients: triangles are used for H<sub>2</sub>O at 50 °C, squares for D<sub>2</sub>O at 20 °C. The Debye plus Drude-Smith fit is shown in grey in Figure 2 and the residues, which are reported at the top of Figure 2 with vertical bars, are larger than the 95% CI measurement uncertainties (horizontal steps).

By comparing the fit results in Table 1 and Table 2, we notice that the time-constants of the main Debye terms are similar across different fit procedures:  $\tau_1$  is about 8.6 ps for H<sub>2</sub>O at 20 °C, 4.7 ps for H<sub>2</sub>O at 50 °C, and 10.9 ps for D<sub>2</sub>O at 20 °C. These results agree with previous

reports detailing faster time constants when water is heated and slower ones upon deuteration<sup>33–37</sup>. The Drude-Smith scattering times are all substantially shorter than this dominant Debye relaxation and close to 100 fs. In contrast, the plasma frequency varies with temperature and isotopic substitution.

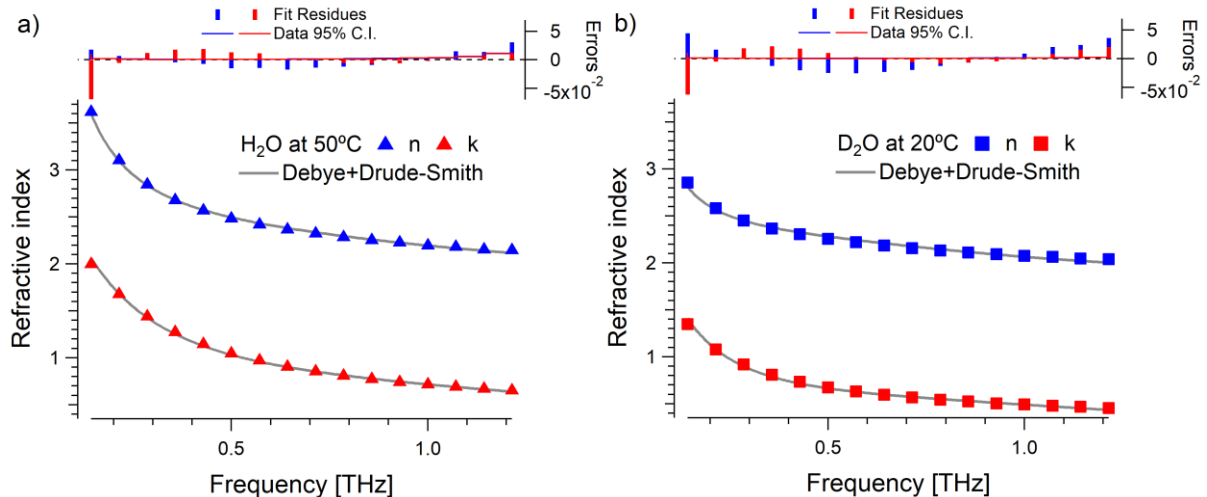


**Figure 2.** Real and imaginary parts of the complex index of refraction of pure H<sub>2</sub>O at 50 °C (a) and of heavy water at 20 °C (b). As expected, when compared to pure water at 20 °C, D<sub>2</sub>O displays a smaller complex refractive index, while heating is associated with a stronger field-matter interaction. The single Debye plus Drude-Smith fit is shown with grey lines. The fit residues are reported by vertical bars in the top panel. The 95% CI from the measurements are reported with horizontal segments and are smaller than the fit residues.

In a conventional Drude model,  $\omega_p^2$  is proportional to the density of carriers. In the present context this microscopic interpretation is not appropriate, because pure liquid water is a large band-gap insulator and does not support long-range electronic transport (i.e., it is an electronic insulator). We therefore use  $\omega_p^2$  only as the effective spectral weight of the localised Drude-Smith component. From the values listed in Table 2, we note that this quantity increases by  $\frac{\omega_p^2(50^\circ\text{C}) - \omega_p^2(20^\circ\text{C})}{\omega_p^2(20^\circ\text{C})} \approx +(18 \pm 8)\%$  in water at 50 °C with respect to water at 20 °C, and decreases by  $\frac{\omega_p^2(\text{D}_2\text{O}) - \omega_p^2(\text{H}_2\text{O})}{\omega_p^2(\text{H}_2\text{O})} \approx -(10 \pm 4)\%$  when comparing D<sub>2</sub>O at 20 °C with H<sub>2</sub>O at 20 °C.

Because hydrogen bonds in water involve donor-acceptor charge transfer and intermolecular charge redistribution, donor/acceptor-imbalanced environments are expected to exhibit asymmetric charge redistribution<sup>1,4–7,11,12</sup>. We therefore searched for an empirical correlation between the Drude-Smith spectral weight and the population of water molecules having unequal numbers of donated and accepted hydrogen bonds. To this end, we performed dedicated neural-network-based molecular dynamics simulations with a deep potential model trained on accurate M06-2X data and developed in Ref.<sup>56</sup>, and classified each instantaneous molecular environment by the number of donated and accepted hydrogen bonds. The isotope comparison was evaluated by performing simulations within the path integral formalism recently introduced by Car and co-workers<sup>57</sup> both for H<sub>2</sub>O and D<sub>2</sub>O at 20 °C. Furthermore,

the temperature dependence was assessed using MB-pol simulations. Full simulation details and hydrogen-bond population tables are provided in the SI.

According to the path integral deep potential molecular dynamics (PI-DPMD) simulation results that include nuclear quantum effects, the amount of water molecules with an uneven number of donated and accepted HBs drops by  $-13.6\%$  when comparing  $D_2O$  at  $20\text{ }^\circ\text{C}$  with  $H_2O$  at  $20\text{ }^\circ\text{C}$ . This agrees within uncertainties with the experimental Drude-Smith estimate,  $-(10 \pm 4)\%$ . According to simulation results of pure water at different temperatures (MB-pol), the fraction of water molecules with an HB imbalance increases by  $+21.9\%$  when comparing  $H_2O$  at  $57\text{ }^\circ\text{C}$  with  $H_2O$  at  $17\text{ }^\circ\text{C}$ , which corroborates the experimental Drude-Smith estimate of  $+(18 \pm 8)\%$ . This correlation is significant because previous attempts with an additional Debye component have not provided consistent trends across temperature and isotope changes. See, for example, Figure 3 in ref. <sup>36</sup> and Figure 2 in ref. <sup>37</sup>.

To clarify the microscopic nature of the terahertz response of liquid water, we performed *ab-initio*-based simulations using the MB-pol model to calculate the imaginary part of the dielectric function of  $H_2O$  at  $57\text{ }^\circ\text{C}$ . The results are shown in Figure 3. The simulations were performed either using a fixed partial-charge dipole approximation, which excludes explicit electronic polarisation and charge redistribution from the dipole definition, or using a neural network trained to reproduce the molecular dipole moment based on a Wannier-centre approach, in which nuclear motion, electronic polarisation, and intermolecular charge redistribution are all included by construction. These results are shown by the red and blue curves in Figure 3a for the partial-charge and Wannier-centre approaches, respectively.

The green curve in Figure 3b corresponds to the difference between the Wannier-centre and fixed-charge spectra. This difference highlights the part of the dielectric response that is not captured by the fixed-charge dipole approximation alone, i.e., it highlights explicit electronic-polarisation, charge-redistribution effects, and nuclear-electronic cross-correlation terms. If such a difference is positive at any given frequency, then there are electronic dynamics that change the total dipole moment at that frequency, with a contribution that exceeds the one of nuclear motions alone. Conversely, if the difference between the Wannier-centre and fixed-charge spectra is smaller than zero, then negative cross-correlations are present, i.e., opposite motions between nuclear and electronic degrees of freedom.

By inspecting Figure 3b, broad translational and librational features are evident around  $\sim 5\text{ THz}$  and  $17\text{ THz}$ , respectively. This is expected, because polarisation effects are known to be relevant for these intermolecular hydrogen-bond-network modes <sup>8-10</sup>. Importantly, the purple-shaded area in Figure 3b highlights a non-zero difference between about  $0.1$  and  $1\text{ THz}$ , roughly overlapping with the empirical Drude-Smith fit. These simulations therefore support the notion that explicit electronic polarisation and intermolecular charge redistribution contribute to the low-frequency THz response of liquid water. In particular, anticorrelated nuclear-electronic motions are expected in the  $\sim 0.1-1\text{ THz}$  band, because the difference signal is negative at those frequencies. The microscopic origin of this band is mixed rather than purely electronic: the fixed-charge spectrum in Figure 3a (red curve) is similar to the experimental response <sup>33,58</sup>

(black) in the same  $\sim 0.1$ -1 THz frequency range, indicating that nuclear motions also contribute.

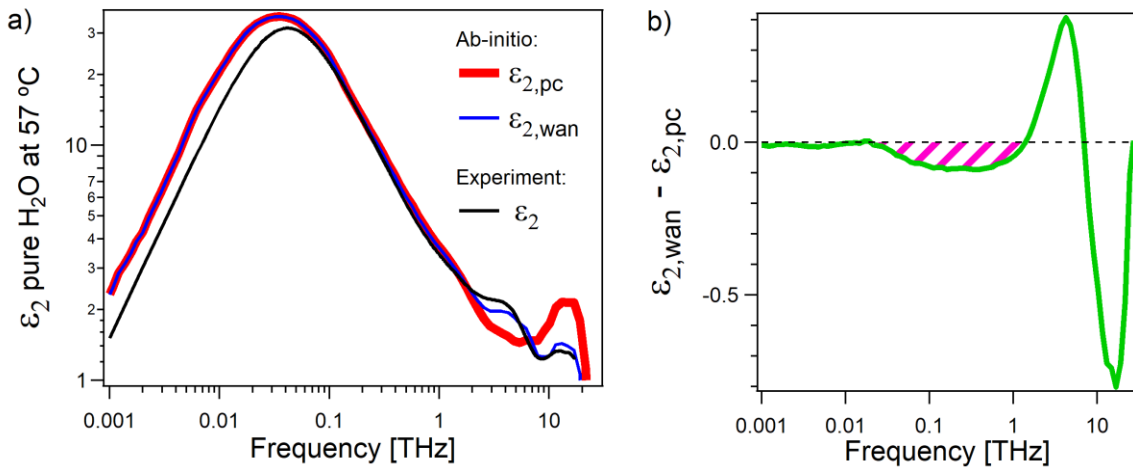


**Figure 3.** Imaginary part of the dielectric function of liquid water over a broadband terahertz spectral range. a) Comparison between established literature experimental results (black) and *ab initio* calculations with either both nuclear and electronic contributions ( $\epsilon_{2,\text{wan}}$  in blue) or a fixed partial-charge dipole approximation, which excludes explicit electronic-polarisation and charge-redistribution effects from the dipole definition ( $\epsilon_{2,\text{pc}}$  in red). b) The green trace shows the difference between the Wannier-centre and fixed-charge spectra, highlighting the part of the response not captured by the fixed-charge dipole approximation. This difference deviates from zero above about 0.03 THz, with a noticeable signal between about 0.1 and 1 THz that is highlighted by the purple shaded area. Large deviations are found in the stretch and libration regions around  $\sim 5$  and 17 THz, respectively.

In conclusion, we investigated the low-frequency dielectric response of liquid water in the terahertz range by comparing the standard double-Debye approach with a model combining one Debye relaxation and one Drude-Smith contribution with strongly localised transport. Both approaches reproduce the main experimental features of the dielectric response of water between about 0.14 and 1.21 THz with comparable fit residuals. However, the Drude-Smith formalism allows for a complementary physical interpretation of water electrodynamics.

The main Debye relaxation times are slower in heavy water and faster upon heating, which is qualitatively consistent with recent *ab initio* results that associate the 8-10 ps Debye-type reorientation response to cross-dipolar correlations involving the orientations of multiple water molecules<sup>48,49</sup>. Importantly, the squared plasma frequency of the Drude-Smith fit correlates with the simulated population of water molecules having unequal numbers of donated and accepted hydrogen bonds. In fact, upon either deuteration or heating, the Drude-Smith spectral-weight changes have the same sign and comparable magnitude as the simulated changes in the donor/acceptor-imbalanced population.

Taken together, these results indicate that transient intermolecular charge redistribution associated with hydrogen-bond-network disorder can contribute to the low-frequency terahertz response of water. The Drude-Smith approach has both an intuitive microscopic interpretation linked to charge localisation, which is corroborated by molecular dynamics simulations

quantifying the amount of water molecules characterized by an imbalance in donating versus accepting HBs, and, importantly, a simple analytical form. This practical approach could therefore complement standard double-Debye procedures and, in some cases, provide deeper microscopic insights. This interpretation overlaps in part with previous suggestions by Popov *et al.*<sup>59</sup>, wherein the dielectric response of water is attributed to the migration of bifurcated hydrogen-bond defects; with the ideas of Artemov *et al.*<sup>60,61</sup>, in which charge fluctuations contribute to the dielectric response of water; and with the proposal by Yada *et al.*<sup>36</sup> of collision processes in non-HB dynamic microstructures.

Finally, dedicated *ab-initio*-based calculations of the full spectral response of water provided a more complete picture: both the nuclear-motion contribution within a fixed-charge dipole approximation and dynamic charge fluctuations, including polarization effects and charge transfer redistributions, are simultaneously present in the low-frequency terahertz response of water. The low-frequency excess response over the experimentally probed range should therefore be regarded as a mixed nuclear-electronic dielectric response, rather than a purely reorientational or electronic process.

## Acknowledgements

FN acknowledges financial support by the DFG (509442914), University of Southampton (Startup package), and Ruhr University Bochum (Novizenprämie, RDSS). AAH acknowledges the funding received by the European Research Council (ERC) under the European Union's Horizon 2020 research and innovation program (Grant No. 101043272 - HyBOP). The views and opinions expressed are those of the authors only and do not necessarily reflect those of the European Union or the European Research Council Executive Agency. Neither the European Union nor the granting authority can be held responsible for them. GC is thankful to CINECA for awards under the ISCRA initiative, for the availability of high-performance computing resources and support.

## References

- (1) Arunan, E.; Desiraju, G. R.; Klein, R. A.; Sadlej, J.; Scheiner, S.; Alkorta, I.; Clary, D. C.; Crabtree, R. H.; Dannenberg, J. J.; Hobza, P.; Kjaergaard, H. G.; Legon, A. C.; Mennucci, B.; Nesbitt, D. J. Definition of the Hydrogen Bond (IUPAC Recommendations 2011). *Pure and Applied Chemistry* **2011**, *83* (8), 1637–1641. <https://doi.org/10.1351/PAC-REC-10-01-02>.
- (2) Chamarro-Contreras, A.; Lopez-Revelo, Y.; Cardenas-Gamboa, J.; Terencio, T. Insights into the Effect of Charges on Hydrogen Bonds. *Int. J. Mol. Sci.* **2024**, *25* (3), 1613. <https://doi.org/10.3390/ijms25031613>.
- (3) Lee, A. J.; Rick, S. W. The Effects of Charge Transfer on the Properties of Liquid Water. *Journal of Chemical Physics* **2011**, *134* (18). <https://doi.org/10.1063/1.3589419>.

- (4) Ojha, D.; Karhan, K.; Kühne, T. D. On the Hydrogen Bond Strength and Vibrational Spectroscopy of Liquid Water. *Sci. Rep.* **2018**, *8* (1). <https://doi.org/10.1038/s41598-018-35357-9>.
- (5) Ben-Amotz, D. Electric Buzz in a Glass of Pure Water. *Science* **2022**, *376* (6595), 800–801. <https://doi.org/10.1126/science.abo3398>.
- (6) Schran, C.; Marsalek, O.; Markland, T. E. Unravelling the Influence of Quantum Proton Delocalization on Electronic Charge Transfer through the Hydrogen Bond. *Chem. Phys. Lett.* **2017**, *678*, 289–295. <https://doi.org/10.1016/j.cplett.2017.04.034>.
- (7) Kumar, R.; Schmidt, J. R.; Skinner, J. L. Hydrogen Bonding Definitions and Dynamics in Liquid Water. *Journal of Chemical Physics* **2007**, *126* (20). <https://doi.org/10.1063/1.2742385>.
- (8) Ito, H.; Hasegawa, T.; Tanimura, Y. Effects of Intermolecular Charge Transfer in Liquid Water on Raman Spectra. *Journal of Physical Chemistry Letters* **2016**, *7* (20), 4147–4151. <https://doi.org/10.1021/acs.jpcllett.6b01766>.
- (9) Torii, H. Intermolecular Electron Density Modulations in Water and Their Effects on the Far-Infrared Spectral Profiles at 6 THz. *Journal of Physical Chemistry B* **2011**, *115* (20), 6636–6643. <https://doi.org/10.1021/jp201695b>.
- (10) Torii, H. Cooperative Contributions of the Intermolecular Charge Fluxes and Intramolecular Polarizations in the Far-Infrared Spectral Intensities of Liquid Water. *J. Chem. Theory Comput.* **2014**, *10* (3), 1219–1227. <https://doi.org/10.1021/ct4011147>.
- (11) Flór, M.; Wilkins, D. M.; de la Puente, M.; Laage, D.; Cassone, G.; Hassanali, A.; Roke, S. Dissecting the Hydrogen Bond Network of Water: Charge Transfer and Nuclear Quantum Effects. *Science* **2024**, *386* (6726). <https://doi.org/10.1126/science.ads4369>.
- (12) Amadeo, A.; Torre, M. F.; Mrázíková, K.; Saija, F.; Trusso, S.; Xie, J.; Tommasini, M.; Cassone, G. Hydrogen Bonds under Electric Fields with Quantum Accuracy. *J. Phys. Chem. A* **2025**, *129* (18), 4077–4092. <https://doi.org/10.1021/ACS.JPCA.5C01095>.
- (13) Ge, X.; Lu, D. Molecular Polarizability of Water from Local Dielectric Response Theory. *Phys. Rev. B* **2017**, *96* (7), 075114. <https://doi.org/10.1103/PhysRevB.96.075114>.
- (14) Pullanchery, S.; Kulik, S.; Rehl, B.; Hassanali, A.; Roke, S. Charge Transfer across C–H···O Hydrogen Bonds Stabilizes Oil Droplets in Water. *Science* **2021**, *374* (6573), 1366–1370. <https://doi.org/10.1126/science.abj3007>.
- (15) Poli, E.; Jong, K. H.; Hassanali, A. Charge Transfer as a Ubiquitous Mechanism in Determining the Negative Charge at Hydrophobic Interfaces. *Nat. Commun.* **2020**, *11* (1). <https://doi.org/10.1038/s41467-020-14659-5>.
- (16) Gasparotto, P.; Hassanali, A. A.; Ceriotti, M. Probing Defects and Correlations in the Hydrogen-Bond Network of Ab Initio Water. *J. Chem. Theory Comput.* **2016**, *12* (4), 1953–1964. <https://doi.org/10.1021/acs.jctc.5b01138>.
- (17) Wang, Z.; Chen, Z.; Fang, J.; Li, S.; Zhou, W.; Qiu, H. Charge Transfer at Air-Water Interfaces: A Machine Learning Potential-Based Molecular Dynamics Study. *Journal of Chemical Physics* **2025**, *162* (24), 244705. <https://doi.org/10.1063/5.0273607/3350869>.

- (18) Amante, G.; Panzera, F.; Centi, G.; Xie, J.; Hassanali, A.; Saitta, A. M.; Cassone, G. *Interfacial Electric Fields in Water Nanodroplets Are Weakly Dependent on Curvature and PH*; 2026. <http://arxiv.org/abs/2604.14784> (accessed 2026-07-05).
- (19) Takeda, J.; Yoshioka, K.; Minami, Y.; Katayama, I. Nanoscale Electron Manipulation in Metals with Intense THz Electric Fields. *J. Phys. D Appl. Phys.* **2018**, *51* (10), 103001. <https://doi.org/10.1088/1361-6463/aaa8c7>.
- (20) Walther, M.; Cooke, D. G.; Sherstan, C.; Hajar, M.; Freeman, M. R.; Hegmann, F. A. Terahertz Conductivity of Thin Gold Films at the Metal-Insulator Percolation Transition. *Phys. Rev. B* **2007**, *76* (12), 125408. <https://doi.org/10.1103/PhysRevB.76.125408>.
- (21) Shimakawa, K.; Kasap, S. Dynamics of Carrier Transport in Nanoscale Materials: Origin of Non-Drude Behavior in the Terahertz Frequency Range. *Applied Sciences* **2016**, *6* (2), 50. <https://doi.org/10.3390/app6020050>.
- (22) Cocker, T. L.; Titova, L. V.; Fourmaux, S.; Bandulet, H. C.; Brassard, D.; Kieffer, J. C.; El Khakani, M. A.; Hegmann, F. A. Terahertz Conductivity of the Metal-Insulator Transition in a Nanogranular VO<sub>2</sub> Film. *Appl. Phys. Lett.* **2010**, *97* (22). <https://doi.org/10.1063/1.3518482>.
- (23) Li, G.; Li, D.; Jin, Z.; Ma, G. Photocarriers Dynamics in Silicon Wafer Studied with Optical-Pump Terahertz-Probe Spectroscopy. *Opt. Commun.* **2012**, *285* (20), 4102–4106. <https://doi.org/10.1016/j.optcom.2012.05.053>.
- (24) Tsokkou, D.; Othonos, A.; Zervos, M. Carrier Dynamics and Conductivity of SnO<sub>2</sub> Nanowires Investigated by Time-Resolved Terahertz Spectroscopy. *Appl. Phys. Lett.* **2012**, *100* (13). <https://doi.org/10.1063/1.3698097>.
- (25) Ahn, H.; Ku, Y.-P.; Wang, Y.-C.; Chuang, C.-H.; Gwo, S.; Pan, C.-L. Terahertz Spectroscopic Study of Vertically Aligned InN Nanorods. *Appl. Phys. Lett.* **2007**, *91* (16). <https://doi.org/10.1063/1.2800292>.
- (26) Lovrinčić, R.; Pucci, A. Infrared Optical Properties of Chromium Nanoscale Films with a Phase Transition. *Phys. Rev. B* **2009**, *80* (20), 205404. <https://doi.org/10.1103/PhysRevB.80.205404>.
- (27) Cooke, D. G.; MacDonald, A. N.; Hryciw, A.; Wang, J.; Li, Q.; Meldrum, A.; Hegmann, F. A. Transient Terahertz Conductivity in Photoexcited Silicon Nanocrystal Films. *Phys. Rev. B* **2006**, *73* (19), 193311. <https://doi.org/10.1103/PhysRevB.73.193311>.
- (28) Kim, J.; Maeng, I.; Jung, J.; Song, H.; Son, J.-H.; Kim, K.; Lee, J.; Kim, C.-H.; Chae, G.; Jun, M.; Hwang, Y.; Jeong Lee, S.; Myoung, J.-M.; Choi, H. Terahertz Time-Domain Measurement of Non-Drude Conductivity in Silver Nanowire Thin Films for Transparent Electrode Applications. *Appl. Phys. Lett.* **2013**, *102* (1). <https://doi.org/10.1063/1.4773179>.
- (29) Smith, N. Classical Generalization of the Drude Formula for the Optical Conductivity. *Phys. Rev. B* **2001**, *64* (15), 155106. <https://doi.org/10.1103/PhysRevB.64.155106>.
- (30) Cocker, T. L.; Baillie, D.; Buruma, M.; Titova, L. V.; Sydora, R. D.; Marsiglio, F.; Hegmann, F. A. Microscopic Origin of the Drude-Smith Model. *Phys. Rev. B* **2017**, *96* (20), 205439. <https://doi.org/10.1103/PhysRevB.96.205439>.

- (31) Kužel, P.; Němec, H. Terahertz Spectroscopy of Nanomaterials: A Close Look at Charge-Carrier Transport. *Adv. Opt. Mater.* **2020**, *8* (3).  
<https://doi.org/10.1002/adom.201900623>.
- (32) Chen, W. C.; Marcus, R. A. The Drude-Smith Equation and Related Equations for the Frequency-Dependent Electrical Conductivity of Materials: Insight from a Memory Function Formalism. *ChemPhysChem* **2021**, *22* (16), 1667–1674.  
<https://doi.org/10.1002/cphc.202100299>.
- (33) Rønne, C.; Keiding, S. R. Low Frequency Spectroscopy of Liquid Water Using THz-Time Domain Spectroscopy. *J. Mol. Liq.* **2002**, *101* (1–3), 199–218.  
[https://doi.org/10.1016/S0167-7322\(02\)00093-4](https://doi.org/10.1016/S0167-7322(02)00093-4).
- (34) Rønne, C.; Åstrand, P.-O.; Keiding, S. R. THz Spectroscopy of Liquid H<sub>2</sub>O and D<sub>2</sub>O. *Phys. Rev. Lett.* **1999**, *82* (14), 2888–2891.  
<https://doi.org/10.1103/PhysRevLett.82.2888>.
- (35) Liebe, H. J.; Hufford, G. A.; Manabe, T. A Model for the Complex Permittivity of Water at Frequencies below 1 THz. *Int. J. Infrared Millimeter Waves* **1991**, *12* (7), 659–675. <https://doi.org/10.1007/BF01008897>.
- (36) Yada, H.; Nagai, M.; Tanaka, K. Origin of the Fast Relaxation Component of Water and Heavy Water Revealed by Terahertz Time-Domain Attenuated Total Reflection Spectroscopy. *Chem. Phys. Lett.* **2008**, *464* (4–6), 166–170.  
<https://doi.org/10.1016/j.cplett.2008.09.015>.
- (37) Kutus, B.; Shalit, A.; Hamm, P.; Hunger, J. Dielectric Response of Light, Heavy and Heavy-Oxygen Water: Isotope Effects on the Hydrogen-Bonding Network's Collective Relaxation Dynamics. *Physical Chemistry Chemical Physics* **2021**, *23* (9), 5467–5473.  
<https://doi.org/10.1039/d0cp06460b>.
- (38) Buchner, R.; Barthel, J.; Stauber, J. The Dielectric Relaxation of Water between 0°C and 35°C. *Chem. Phys. Lett.* **1999**, *306* (1–2), 57–63. [https://doi.org/10.1016/S0009-2614\(99\)00455-8](https://doi.org/10.1016/S0009-2614(99)00455-8).
- (39) Ellison, W. J. Permittivity of Pure Water, at Standard Atmospheric Pressure, over the Frequency Range –25THz and the Temperature Range –100°C. *J. Phys. Chem. Ref. Data* **2007**, *36* (1), 1–18. <https://doi.org/10.1063/1.2360986>.
- (40) Shiraga, K.; Tanaka, K.; Arikawa, T.; Saito, S.; Ogawa, Y. Reconsideration of the Relaxational and Vibrational Line Shapes of Liquid Water Based on Ultrabroadband Dielectric Spectroscopy. *Physical Chemistry Chemical Physics* **2018**, *20* (41), 26200–26209. <https://doi.org/10.1039/c8cp04778b>.
- (41) Elton, D. C. The Origin of the Debye Relaxation in Liquid Water and Fitting the High Frequency Excess Response. *Physical Chemistry Chemical Physics* **2017**, *19* (28), 18739–18749. <https://doi.org/10.1039/c7cp02884a>.
- (42) Lunkenheimer, P.; Emmert, S.; Gulich, R.; Köhler, M.; Wolf, M.; Schwab, M.; Loidl, A. Electromagnetic-Radiation Absorption by Water. *Phys. Rev. E* **2017**, *96* (6), 062607.  
<https://doi.org/10.1103/PhysRevE.96.062607>.
- (43) Fukasawa, T.; Sato, T.; Watanabe, J.; Hama, Y.; Kunz, W.; Buchner, R. Relation between Dielectric and Low-Frequency Raman Spectra of Hydrogen-Bond Liquids.

- Phys. Rev. Lett.* **2005**, *95* (19), 197802.  
<https://doi.org/10.1103/PhysRevLett.95.197802>.
- (44) Vinh, N. Q.; Sherwin, M. S.; Allen, S. J.; George, D. K.; Rahmani, A. J.; Plaxco, K. W. High-Precision Gigahertz-to-Terahertz Spectroscopy of Aqueous Salt Solutions as a Probe of the Femtosecond-to-Picosecond Dynamics of Liquid Water. *J. Chem. Phys.* **2015**, *142* (16), 164502. <https://doi.org/10.1063/1.4918708>.
- (45) Penkov, N.; Shvirst, N.; Yashin, V.; Fesenko, E. Terahertz Spectroscopy Applied for Investigation of Water Structure. *Journal of Physical Chemistry B* **2015**, *119* (39), 12664–12670. <https://doi.org/10.1021/acs.jpccb.5b06622>.
- (46) Adams, E. M.; Hao, H.; Leven, I.; Rüttermann, M.; Wirtz, H.; Havenith, M.; Head-Gordon, T. Proton Traffic Jam: Effect of Nanoconfinement and Acid Concentration on Proton Hopping Mechanism. *Angewandte Chemie* **2021**, *133* (48), 25623–25631. <https://doi.org/10.1002/ANGE.202108766>.
- (47) Sebastiani, F.; Wolf, S. L. P.; Born, B.; Luong, T. Q.; Cölfen, H.; Gebauer, D.; Havenith, M. Water Dynamics from THz Spectroscopy Reveal the Locus of a Liquid–Liquid Binodal Limit in Aqueous CaCO<sub>3</sub> Solutions. *Angew. Chem. Int. Ed.* **2017**, *56* (2), 490–495. <https://doi.org/10.1002/anie.201610554>.
- (48) Hölzl, C.; Forbert, H.; Marx, D. Dielectric Relaxation of Water: Assessing the Impact of Localized Modes, Translational Diffusion, and Collective Dynamics. *Physical Chemistry Chemical Physics* **2021**, *23* (37), 20875–20882. <https://doi.org/10.1039/d1cp03507j>.
- (49) Pabst, F.; Baroni, S. How Salt Solvation Slows Water Dynamics While Blue-Shifting Its Dielectric Spectrum. *J. Phys. Chem. Lett.* **2025**, 7915–7920. <https://doi.org/10.1021/acs.jpcclett.5c01401>.
- (50) Alvarez, F.; Arbe, A.; Colmenero, J. The Debye’s Model for the Dielectric Relaxation of Liquid Water and the Role of Cross-Dipolar Correlations. A MD-Simulations Study. *J. Chem. Phys.* **2023**, *159* (13), 134505. <https://doi.org/10.1063/5.0168588>.
- (51) Novelli, F. Terahertz Spectroscopy of Thick and Diluted Water Solutions. *Opt. Express* **2024**, *32* (7), 11041. <https://doi.org/10.1364/OE.510393>.
- (52) Novelli, F.; Spina, L.; Rubano, A.; Cattaneo, L.; Paparo, D.; Ciuchi, F.; De Santo, M. P. Intense TeraHertz Time Domain Spectroscopy of Water-Based Liquid Crystals. *IEEE Trans. Terahertz Sci. Technol.* **2026**, 1–10. <https://doi.org/10.1109/TTHZ.2026.3690056>.
- (53) Malmberg, C. G. Dielectric Constant of Deuterium Oxide. *J. Res. Natl. Bur. Stand.* **1958**, *60* (6), 609. <https://doi.org/10.6028/jres.060.060>.
- (54) Archer, D. G.; Wang, P. The Dielectric Constant of Water and Debye-Hückel Limiting Law Slopes. *J. Phys. Chem. Ref. Data* **1990**, *19* (2), 371–411. <https://doi.org/10.1063/1.555853>.
- (55) Vidulich, G. A.; Evans, D. F.; Kay, R. L. The Dielectric Constant of Water and Heavy Water between 0 and 40°. *J. Phys. Chem.* **1967**, *71* (3), 656–662. <https://doi.org/10.1021/j100862a028>.

- (56) Zhang, P.; Xu, X. Propensity of Water Self-Ions at Air(Oil)–Water Interfaces Revealed by Deep Potential Molecular Dynamics with Enhanced Sampling. *Langmuir* **2025**, *41* (5), 3675–3683. <https://doi.org/10.1021/ACS.LANGMUIR.4C05004>.
- (57) Li, Y.; Gomez, A.; Cai, K.; Zhang, C.; Fu, L.; Jia, W.; Feldman, Y. M. Y.; Blumer, O.; Higer, J.; Hirshberg, B.; Xu, S.; Kohlmeyer, A.; Car, R. Fix Pimd/Langevin: An Efficient Implementation of Path Integral Molecular Dynamics in LAMMPS. *J. Chem. Phys.* **2026**, *164* (14), 144119. <https://doi.org/10.1063/5.0328429/3386874>.
- (58) Zelsmann, H. R. Temperature Dependence of the Optical Constants for Liquid H<sub>2</sub>O and D<sub>2</sub>O in the Far IR Region. *J. Mol. Struct.* **1995**, *350* (2), 95–114. [https://doi.org/10.1016/0022-2860\(94\)08471-S](https://doi.org/10.1016/0022-2860(94)08471-S).
- (59) Popov, I.; Ishai, P. Ben; Khamzin, A.; Feldman, Y. The Mechanism of the Dielectric Relaxation in Water. *Physical Chemistry Chemical Physics* **2016**, *18* (20), 13941–13953. <https://doi.org/10.1039/C6CP02195F>.
- (60) Artemov, V. G. A Unified Mechanism for Ice and Water Electrical Conductivity from Direct Current to Terahertz. *Physical Chemistry Chemical Physics* **2019**, *21* (15), 8067–8072. <https://doi.org/10.1039/c9cp00257j>.
- (61) Volkov, A. A.; Artemov, V. G.; Pronin, A. V. A Radically New Suggestion about the Electrodynamics of Water: Can the PH Index and the Debye Relaxation Be of a Common Origin? *EPL (Europhysics Letters)* **2014**, *106* (4), 46004. <https://doi.org/10.1209/0295-5075/106/46004>.

## **Supplementary Information**

### **Hydrogen-Bond Donor-Acceptor Imbalance in Low-Frequency Terahertz Water Spectra**

Lilian Najm Alsayed<sup>1</sup>, Florian Pabst<sup>2</sup>, Giuseppe Cassone<sup>3</sup>, Ali Hassanali<sup>2</sup>, Fabio Novelli<sup>1,\*</sup>

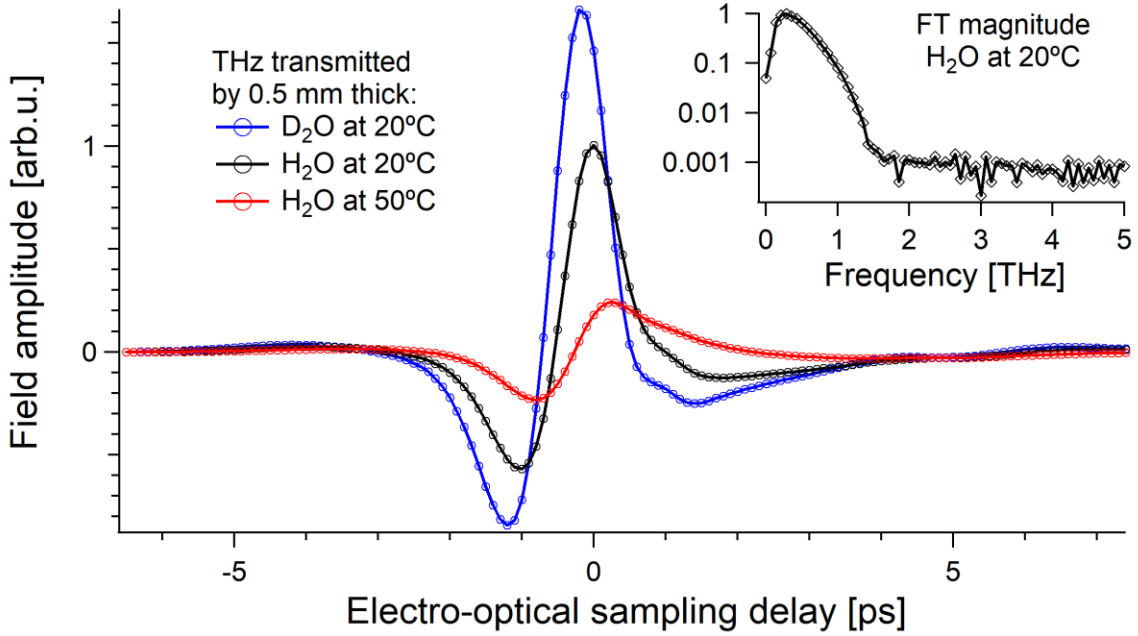
<sup>1</sup>School of Physics and Astronomy, Faculty of Engineering and Physical Sciences, University of Southampton, UK

<sup>2</sup>CMSP, The Abdus Salam Centre for Theoretical Physics, 34151 Trieste, Italy

<sup>3</sup>Institute for Chemical-Physical Processes, National Research Council of Italy, viale Ferdinando Stagno d'Alcontres 37, 98158 Messina, Italy

\*F.Novelli@soton.ac.uk

**Experiments.** Terahertz radiation was generated by tilted-front optical rectification of  $\sim 90$ -fs long titanium-sapphire amplified pulses in a lithium niobate prism. The transmission by the opaque samples was detected via electro-optical sampling in a 1 mm thick zinc telluride crystal, over a 13.9 ps temporal range, and in steps of 0.1 ps. The acquisition of one THz trace took about 20 seconds and was repeated 15 times. Uncertainties from these repetitions were estimated to a 95% confidence interval (CI). The samples were mounted in a static liquid cell with 0.5 mm thick diamond windows, a 0.5 mm Teflon spacer, and attached to a recirculating chiller stabilising the temperature within  $\pm 0.05$  °C. Pure milli-Q liquid water at  $20 \pm 0.05$  °C was used as reference, see the black curve in Supplementary Figure 1. The corresponding magnitude spectrum spans between about 0.14 and 1.21 THz with a dynamic range of  $\sim 30$  dB, see the inset in Supplementary Figure 1. We also measured pure milli-Q liquid water at  $50 \pm 0.05$  °C (red in Supplementary Figure 1) and  $>99\%$ -pure  $D_2O$  at  $20 \pm 0.05$  °C (blue).



**Supplementary Figure 1.** Intense time-domain terahertz spectroscopy of water with different hydrogen-bonding strength. The THz field transmitted by a 0.5 mm thick layer of pure water at 20 °C is shown with black circles and the corresponding spectrum is reported in the inset with black diamonds. As shown by the blue THz trace, both absorption and refraction decrease by isotope substitution ( $D_2O$ ). On the contrary, when  $H_2O$  is heated, it becomes more absorptive and refractive. See the red trace that is obtained at the temperature of 50 °C. The 95% confidence interval errors calculated from 15 measurements are plotted together with each THz trace, but they are not visible because they are smaller than the line thickness.

The optical properties of these samples were obtained by numerical inversion of eq. 3 in ref. <sup>1</sup>, which reads

$$\frac{E_{\text{sample}}}{E_{\text{wat}}} = \frac{(n_{\text{sample}} + ik_{\text{sample}})(n_{\text{wat}} + ik_{\text{wat}} + 2.37)^2}{(n_{\text{wat}} + ik_{\text{wat}})(n_{\text{sample}} + ik_{\text{sample}} + 2.37)^2} e^{i\frac{\omega d}{c}(n_{\text{sample}} - n_{\text{wat}})} e^{-\frac{\omega d}{c}(k_{\text{sample}} - k_{\text{wat}})} \quad (1)$$

where  $i$  is the imaginary unit,  $E_{sample}$  is the complex and frequency-dependent Fourier-transform (FT) of the THz field transmitted by a sample (H<sub>2</sub>O at 50 °C or D<sub>2</sub>O at 20 °C),  $E_{wat}$  is the FT of the reference (pure H<sub>2</sub>O at 20 °C),  $n_{wat}$  and  $k_{wat}$  are known<sup>1</sup>, 2.37 is the real index of refraction of the diamond windows of the sample holder<sup>1</sup>, and  $n_{sample}$  ( $k_{sample}$ ) is the sought index of refraction (extinction coefficient). Further details on stability, repeatability, and data analysis of inTHz-TDS can be found in ref.<sup>1,2</sup>.

**Data analysis.** The real and imaginary parts of the index of refraction were calculated from the known relationships  $n = \frac{1}{\sqrt{2}}\sqrt{\varepsilon_1 + \sqrt{\varepsilon_1^2 + \varepsilon_2^2}}$  and  $k = \frac{1}{\sqrt{2}}\sqrt{-\varepsilon_1 + \sqrt{\varepsilon_1^2 + \varepsilon_2^2}}$ , respectively. For the double-Debye, the following functions were used to simultaneously fit the real and imaginary parts of the complex dielectric function:

$$\varepsilon_1(\omega) = \varepsilon_\infty + \frac{\Delta\varepsilon_1}{1+\omega^2\tau_1^2} + \frac{\Delta\varepsilon_2}{1+\omega^2\tau_2^2} \quad (2)$$

$$\varepsilon_2(\omega) = \frac{\Delta\varepsilon_1\omega\tau_1}{1+\omega^2\tau_1^2} + \frac{\Delta\varepsilon_2\omega\tau_2}{1+\omega^2\tau_2^2} \quad (3)$$

with  $\nu = \frac{\omega}{2\pi}$  frequency,  $\varepsilon_\infty$  dielectric constant at higher frequencies,  $\Delta\varepsilon_1$  and  $\Delta\varepsilon_2$  the weights of the Debye-type reorientations with time-constants equal to  $\tau_1$  and  $\tau_2$ , respectively. The values of  $\Delta\varepsilon_1$  and  $\Delta\varepsilon_2$  are constrained by the boundary conditions of the dielectric function:  $\varepsilon_S = \lim_{\omega \rightarrow 0} [\varepsilon_1(\omega) + i\varepsilon_2(\omega)]$  and  $\varepsilon_\infty = \lim_{\omega \rightarrow \infty} [\varepsilon_1(\omega) + i\varepsilon_2(\omega)]$ . These limits imply  $\Delta\varepsilon_1 = \varepsilon_S - \varepsilon_d$  and  $\Delta\varepsilon_2 = \varepsilon_d - \varepsilon_\infty$ , where the static dielectric constant  $\varepsilon_S$  was fixed to literature values<sup>3-5</sup>, and  $\varepsilon_d$  is the first Debye term.

For the Debye plus Drude-Smith fit, the following functions were used:

$$\varepsilon_1(\omega) = \varepsilon_\infty + \frac{\Delta\varepsilon'_1}{1+\omega^2\tau_1^2} - \frac{\omega_p^2\tau^2(1+\omega^2\tau^2+2c)}{(1+\omega^2\tau^2)^2} \quad (4)$$

$$\varepsilon_2(\omega) = \frac{\Delta\varepsilon'_1\omega\tau_1}{1+\omega^2\tau_1^2} + \frac{\omega_p^2\tau[1+\omega^2\tau^2+c(1-\omega^2\tau^2)]}{\omega(1+\omega^2\tau^2)^2} \quad (5)$$

including the additional parameters  $c = -1$ , used here as an effective localisation parameter for a non-propagating charge-redistribution response,  $\omega_p$  effective spectral weight parameter, and  $\tau$  effective scattering time. The strength of the Debye term is determined by the parameter  $\Delta\varepsilon'_1$  and constrained by the limiting values of the dielectric function for static and high-frequency fields. By rearranging the identity  $\varepsilon_S = \varepsilon_1(0) = \varepsilon_\infty + \Delta\varepsilon'_1 - \omega_p^2\tau^2(1+2c)$ , we obtain  $\Delta\varepsilon'_1 = \varepsilon_S - \varepsilon_\infty - \omega_p^2\tau^2$  for  $c = -1$ .

As pure liquid water does not support long-range electronic transport, only the fully localised, zero dc electronic conductivity limit of the Drude-Smith expression is physically acceptable. We therefore fixed  $c = -1$ . This also ensured that the double-Debye and Debye plus Drude-Smith fit have the same number of free parameters:  $\varepsilon_d, \varepsilon_\infty, \tau_1, \tau_2$  for the double-Debye;  $\varepsilon_\infty, \tau_1, \omega_p, \tau$  for the Debye plus Drude-Smith.

**Simulations.** Neural-network-based molecular dynamics simulations were carried out with the LAMMPS software (v. 29Aug2024)<sup>6</sup>. We did not develop our own model and the reactive

deep potential trained on the hybrid meta-GGA M06-2X<sup>7</sup> exchange and correlation functional reported in Ref.<sup>8</sup> was employed. For more details, the interested reader can refer to the dedicated repository for information on the training dataset – which includes neutral bulk water, bulk water containing water counterions, air-water interfaces – and relevant validation<sup>8,9</sup>. 256 H<sub>2</sub>O and 256 D<sub>2</sub>O molecules were arranged in cubic boxes with edges of 19.641 Å to reproduce a liquid density of 1.0 g/cm<sup>3</sup>.

Standard deep potential molecular dynamics (DPMD) with classical nuclei and path integral DPMD simulations including Nuclear Quantum Effects were performed on both systems, leading to four (PI-)DPMD simulations. Whereas DPMD simulations were run for 1 ns each, PI-DPMD were executed for 500 ps each only. This was dictated by the increased computational effort introduced by the simulation of 16 different replicas via the recently developed efficient fix pimd/langevin implementation of PIMD<sup>10</sup>. Furthermore, a smaller timestep of 0.25 fs was used in PI-DPMD simulations whereas a timestep of 1 fs was selected for the classical nuclei DPMD ones, as usual. All (PI-)DPMD simulations were executed in the canonical NVT ensemble at a target temperature of 298 K.

**Supplementary Table 1.** Deuteration effects: simulation results from DPMD and PI-DPMD calculations. The configurations of the water molecules are reported as a function of the number of donated (D) and accepted (A) hydrogen-bonds (HB).

HB configuration	DPMD		PI-DPMD	
	H <sub>2</sub> O at 20 °C	D <sub>2</sub> O at 20 °C	H <sub>2</sub> O at 20 °C	D <sub>2</sub> O at 20 °C
0D0A	6.445E-05	5.840E-05	1.555E-04	7.805E-05
0D1A	5.700E-04	5.508E-04	9.417E-04	5.669E-04
0D2A	3.721E-04	3.703E-04	9.375E-04	4.433E-04
0D3A	6.562E-06	5.586E-06	6.250E-05	9.765E-06
0D4A	7.810E-08	1.172E-07	1.562E-07	2.344E-07
1D0A	3.892E-04	3.428E-04	1.238E-03	4.060E-04
1D1A	1.430E-02	1.332E-02	2.465E-02	1.400E-02
1D2A	3.446E-02	3.410E-02	5.403E-02	4.080E-02
1D3A	8.614E-04	7.903E-04	2.125E-03	1.004E-03
1D4A	3.828E-06	1.953E-06	8.437E-06	6.016E-06
2D0A	6.890E-04	5.799E-04	1.990E-03	7.991E-04
2D1A	7.552E-02	7.403E-02	8.967E-02	7.864E-02
2D2A	8.268E-01	8.311E-01	7.834E-01	8.202E-01
2D3A	4.276E-02	4.161E-02	3.723E-02	3.971E-02
2D4A	2.800E-04	2.145E-04	2.336E-04	2.123E-04
2D5A	2.734E-07	2.344E-07	3.125E-07	7.810E-08
3D0A	1.297E-05	1.129E-05	2.234E-05	1.398E-05
3D1A	6.685E-04	6.168E-04	7.768E-04	7.073E-04
3D2A	2.187E-03	2.221E-03	2.492E-03	2.339E-03
3D3A	6.168E-05	6.418E-05	6.609E-05	6.898E-05
3D4A	1.953E-07	3.125E-07	6.250E-07	2.344E-07
4D1A	8.203E-07	7.812E-07	1.719E-06	1.563E-06
4D2A	1.094E-06	7.812E-07	2.344E-06	1.641E-06
Sum D = A	84.41%	84.46%	80.82%	83.43%
Sum D ≠ A	15.88%	15.54%	19.18%	16.57%

Temperature dependent simulations with the MB-pol deep neural network <sup>11</sup> were performed using LAMMPS <sup>6</sup>, interfaced with the DeepMD-kit <sup>12</sup>, on systems of 512 water molecules. First, NPT simulations were performed to equilibrate the system with a time step of 0.5 fs. The density obtained at the end of this simulation was then used for a subsequent NVT equilibration run, again with a 0.5 fs time step. From this run, eight independent configurations were extracted and used as starting points for eight production runs in the NVE ensemble, with a time step of 0.25 fs and a duration of 5 ns at 17 °C and 2 ns at 57 °C.

H-bond statistics were calculated across one NVE production run, employing the 3.5 Å distance criterion between neighbouring oxygens and an H-O---O angle less than 30 degrees.

**Supplementary Table 2.** *Temperature effects: simulation results from the ab-initio-based MB-pol approach. The configurations of the water molecules are reported as a function of the number of donated (D) and accepted (A) hydrogen-bonds (HB).*

<i>HB configuration</i>	MB-pol	
	H <sub>2</sub> O at 17 °C	H <sub>2</sub> O at 57 °C
0D0A	0.00070	0.00186
0D1A	0.00504	0.01063
0D2A	0.00469	0.00969
0D3A	0.00020	0.00055
1D0A	0.00400	0.01000
1D1A	0.05820	0.10311
1D2A	0.10227	0.13131
1D3A	0.00674	0.01184
1D4A	0.00008	0.00020
2D0A	0.00746	0.01461
2D1A	0.17293	0.20252
2D2A	0.56404	0.43539
2D3A	0.06668	0.06064
2D4A	0.00094	0.00117
3D0A	0.00006	0.00012
3D1A	0.00193	0.00209
3D2A	0.00371	0.00389
3D3A	0.00029	0.00039
Sum D = A	62.32%	54.08%
Sum D ≠ A	37.68%	45.92%

Dielectric spectra (imaginary part of the dielectric function) were calculated from the total electric dipole moment  $\mathbf{M}$  of the simulation box, obtained either using a second neural network, trained to predict molecular dipole moments from DFT-based Wannier centre calculations <sup>13</sup>, or by placing fixed charges of +0.5e and -1e on the hydrogen or oxygen atom, respectively, via the equation

$$\epsilon_2(\omega) = \frac{\omega}{3V\epsilon_0k_B T} \int dt e^{-i\omega t} \langle \mathbf{M}(t) \cdot \mathbf{M}(0) \rangle \quad (6)$$

where  $V$  is the box volume,  $\mathbf{M}$  is the total dipole moment of the system (i.e., the sum over all molecular dipole moments),  $T$  is the simulation temperature, and  $\epsilon_0$  and  $k_B$  are the vacuum

permittivity and Boltzmann constant, respectively. The autocorrelation functions of the dipole moment time series from the eight production runs are averaged to reduce the noise of the spectra. To allow for a quantitative comparison between the spectral shapes obtained with the two approaches, a small scaling factor (1.036) was applied to the fixed-charge spectrum to overlap the spectra at the main Debye peak, compensating for the arbitrary absolute dipole magnitude imposed by the fixed partial charges.

The configurations of the water molecules as a function of the number of donated and accepted hydrogen-bonds are reported in Supplementary Table 1 and Supplementary Table 2 for the PI-DPMD and MB-pol simulations, respectively. The amount of tetrahedrally coordinated molecules corresponds to the 2D2A fraction. Because the isotope and temperature trends were obtained using different simulation protocols, we interpreted only relative changes within each protocol.

From Supplementary Table 1, we estimated that deuteration decreases the amount of water molecules with an uneven number of donated and accepted bonds from 19.18% in H<sub>2</sub>O at 20 °C to 16.57% in D<sub>2</sub>O at 20 °C (“Sum D ≠ A” row in Supplementary Table 1). The corresponding variation is  $16.57/19.18 - 1 \sim -13.6\%$ . From Supplementary Table 2, we estimated that varying the temperature of H<sub>2</sub>O from 17 °C to 57 °C increases the fraction of water molecules with an uneven number of accepted and donated bonds from 37.68% to 45.92%. The corresponding variation is  $45.92/37.68 - 1 \sim +21.9\%$ .

## References

- (1) Novelli, F. Terahertz Spectroscopy of Thick and Diluted Water Solutions. *Opt. Express* **2024**, 32 (7), 11041. <https://doi.org/10.1364/OE.510393>.
- (2) Novelli, F.; Spina, L.; Rubano, A.; Cattaneo, L.; Paparo, D.; Ciuchi, F.; De Santo, M. P. Intense TeraHertz Time Domain Spectroscopy of Water-Based Liquid Crystals. *IEEE Trans. Terahertz Sci. Technol.* **2026**, 1–10. <https://doi.org/10.1109/TTHZ.2026.3690056>.
- (3) Malmberg, C. G. Dielectric Constant of Deuterium Oxide. *J. Res. Natl. Bur. Stand.* **1958**, 60 (6), 609. <https://doi.org/10.6028/jres.060.060>.
- (4) Archer, D. G.; Wang, P. The Dielectric Constant of Water and Debye-Hückel Limiting Law Slopes. *J. Phys. Chem. Ref. Data* **1990**, 19 (2), 371–411. <https://doi.org/10.1063/1.555853>.
- (5) Vidulich, G. A.; Evans, D. F.; Kay, R. L. The Dielectric Constant of Water and Heavy Water between 0 and 40°. *J. Phys. Chem.* **1967**, 71 (3), 656–662. <https://doi.org/10.1021/j100862a028>.
- (6) Thompson, A. P.; Aktulga, H. M.; Berger, R.; Bolintineanu, D. S.; Brown, W. M.; Crozier, P. S.; in 't Veld, P. J.; Kohlmeyer, A.; Moore, S. G.; Nguyen, T. D.; Shan, R.; Stevens, M. J.; Tranchida, J.; Trott, C.; Plimpton, S. J. LAMMPS - a Flexible Simulation Tool for Particle-Based Materials Modeling at the Atomic, Meso, and Continuum Scales. *Comput. Phys. Commun.* **2022**, 271, 108171. <https://doi.org/10.1016/J.CPC.2021.108171>.
- (7) Zhao, Y.; Truhlar, D. G.; Zhao, Y.; Truhlar, D. G. The M06 Suite of Density Functionals for Main Group Thermochemistry, Thermochemical Kinetics, Noncovalent Interactions, Excited States, and Transition Elements: Two New Functionals and Systematic Testing of Four M06-

- Class Functionals and 12 Other Functio.... *Theoretical Chemistry Accounts* 2007 120:1 **2007**, 120 (1), 215–241. <https://doi.org/10.1007/S00214-007-0310-X>.
- (8) Zhang, P.; Xu, X. Propensity of Water Self-Ions at Air(Oil)–Water Interfaces Revealed by Deep Potential Molecular Dynamics with Enhanced Sampling. *Langmuir* **2025**, 41 (5), 3675–3683. <https://doi.org/10.1021/ACS.LANGMUIR.4C05004>.
- (9) *GitHub - Zhang-pchao/OilWaterInterface · GitHub*. <https://github.com/Zhang-pchao/OilWaterInterface> (accessed 2026-07-05).
- (10) Li, Y.; Gomez, A.; Cai, K.; Zhang, C.; Fu, L.; Jia, W.; Feldman, Y. M. Y.; Blumer, O.; Higer, J.; Hirshberg, B.; Xu, S.; Kohlmeyer, A.; Car, R. Fix Pimd/Langevin: An Efficient Implementation of Path Integral Molecular Dynamics in LAMMPS. *J. Chem. Phys.* **2026**, 164 (14), 144119. <https://doi.org/10.1063/5.0328429/3386874>.
- (11) Bore, S. L.; Paesani, F. Realistic Phase Diagram of Water from “First Principles” Data-Driven Quantum Simulations. *Nature Communications* 2023 14:1 **2023**, 14 (1), 3349-. <https://doi.org/10.1038/s41467-023-38855-1>.
- (12) Zeng, J.; Zhang, D.; Lu, D.; Mo, P.; Li, Z.; Chen, Y.; Rynik, M.; Huang, L.; Li, Z.; Shi, S.; Wang, Y.; Ye, H.; Tuo, P.; Yang, J.; Ding, Y.; Li, Y.; Tisi, D.; Zeng, Q.; Bao, H.; Xia, Y.; Huang, J.; Muraoka, K.; Wang, Y.; Chang, J.; Yuan, F.; Bore, S. L.; Cai, C.; Lin, Y.; Wang, B.; Xu, J.; Zhu, J. X.; Luo, C.; Zhang, Y.; Goodall, R. E. A.; Liang, W.; Singh, A. K.; Yao, S.; Zhang, J.; Wentzcovitch, R.; Han, J.; Liu, J.; Jia, W.; York, D. M.; Weinan, E.; Car, R.; Zhang, L.; Wang, H. DeePMD-Kit v2: A Software Package for Deep Potential Models. *Journal of Chemical Physics* **2023**, 159 (5), 54801. <https://doi.org/10.1063/5.0155600/2904916>.
- (13) Malosso, C.; Manko, N.; Izzo, M. G.; Baroni, S.; Hassanali, A. Evidence of Ferroelectric Features in Low-Density Supercooled Water from Ab Initio Deep Neural-Network Simulations. *Proceedings of the National Academy of Sciences* **2024**, 121 (32), e2407295121. <https://doi.org/10.1073/pnas.2407295121>.